

Accepted Manuscript

Structure and kinematics of the Sumatran Fault System in North Sumatra
(Indonesia)

David Fernández-Blanco, Melody Philippon, Christoph von Hagke

PII: S0040-1951(16)30120-2
DOI: doi: [10.1016/j.tecto.2016.04.050](https://doi.org/10.1016/j.tecto.2016.04.050)
Reference: TECTO 127089

To appear in: *Tectonophysics*

Received date: 28 September 2015
Revised date: 8 April 2016
Accepted date: 27 April 2016



Please cite this article as: Fernández-Blanco, David, Philippon, Melody, von Hagke, Christoph, Structure and kinematics of the Sumatran Fault System in North Sumatra (Indonesia), *Tectonophysics* (2016), doi: [10.1016/j.tecto.2016.04.050](https://doi.org/10.1016/j.tecto.2016.04.050)

This is a PDF file of an unedited manuscript that has been accepted for publication. As a service to our customers we are providing this early version of the manuscript. The manuscript will undergo copyediting, typesetting, and review of the resulting proof before it is published in its final form. Please note that during the production process errors may be discovered which could affect the content, and all legal disclaimers that apply to the journal pertain.

Tectonics of oblique boundary systems

Structure and kinematics of the Sumatran Fault System in North Sumatra (Indonesia)

David Fernández-Blanco^a, Melody Philippon^b, Christoph von Hagke^c

^a*Institut de Physique du Globe de Paris, Sorbonne Paris Cité, Univ Paris Diderot, CNRS, F-75005 Paris, France*

^b*Université des Antilles, Campus de Fouillole, 97100 Point à Pitre, UMR CNRS 5243, Géosciences Montpellier, 34095 Montpellier*

^c*RWTH Aachen University, Institute of Structural Geology, Tectonics and Geomechanics, Lochnerstraße 4-20, 52056 Aachen, Germany*

Abstract

Lithospheric-scale faults related to oblique subduction are responsible for some of the most hazardous earthquakes reported worldwide. The mega-thrust in the Sunda sector of the Sumatran oblique subduction has been intensively studied, especially after the infamous 2004 Mw 9.1 earthquake, but its onshore kinematic complement within the Sumatran subduction, the transform Sumatran Fault System, has received considerably less attention. In this paper, we apply a combination of analysis of Digital Elevation Models (ASTER GDEM) and field evidence to resolve the kinematics of the leading edge of deformation of the northern sector of the Sumatran Fault System. To this end, we mapped the northernmost tip of Sumatra, including the islands to the northwest, between 4.5° N and 6° N. Here, major topographic highs are related to different faults. Using field evidence and our GDEM structural mapping, we can show that in the area where the fault bifurcates into two fault strands, two independent kinematic regimes evolve, both consistent with the large-scale framework of the Sumatran Fault System. Whereas the eastern branch is a classic Riedel system, the western branch features a fold-and-thrust belt. The latter contractional feature accommodated significant amounts (c. 20%) of shortening of the system in the study area. Our field observations of the tip of the NSFS match a strain pattern with a western contractional domain (Pulau Weh thrust splay) and an eastern extensional domain (Pulau Aceh riedel system), which are together characteristic of the tip of a propagating strike-slip fault, from a mechanical viewpoint. For the first time, we describe the strain partitioning resulting from the propagation of the NSFS in Sumatra mainland. Our study helps understanding complex kinematics of an evolving strike-slip system, and stresses the importance of field studies in addition to remote sensing and geophysical studies.

Crown copyright © 2015 Published by Elsevier Ltd.

Keywords: strike-slip system, slip partitioning, forearc sliver plate, Sumatran Fault System, Sumatra

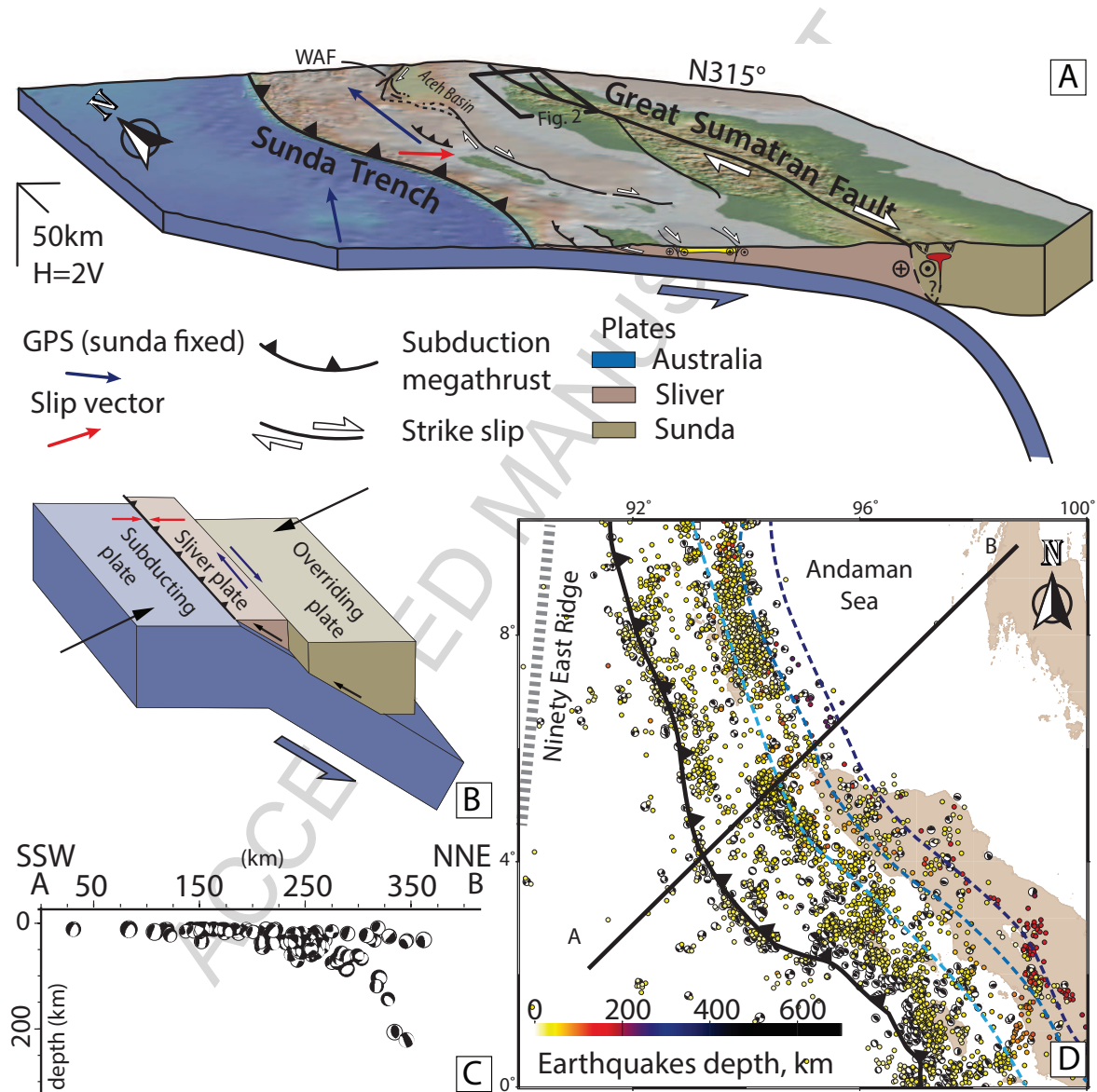


Figure 1. General tectonic context in the Sumatran section of the Sunda forearc. A: Real-scale 3D view of the tectonic configuration of the northern sector of the Sumatran section of the Sunda arc, showing the main regional and tectonic-scale features, as well as GPS and slip vectors. The frontal cross-section transects the Nias island and the Toba caldera in a direction roughly perpendicular to the Sunda Trench and the Sumatran Fault System. Location of the study area (frame of Fig. 2) is also shown. Northern Sumatra off-shore structures are from Martin et al. (2014); WAF stands for West Andaman Fault. B: Idealized block diagram showing the geometry of the sliver plate and overall motions under oblique subduction (modified from McCaffrey (2009) to emphasize correlations with panel A). Cross-section (C) and map view (D) showing the location and depth of earthquakes and their focal mechanisms in the study area and surroundings, after Heuret and Lallemand (2005). Blue dotted lines represent the slab 50 km-isocontours with a color gradient from light to dark with increasing depth (Gudmundsson and Sambridge, 1998).

1. Introduction

Lithospheric-scale strike-slip faults develop worldwide by slip partitioning during oblique convergence between two tectonic plates. These trench-parallel strike-slip faults accommodate margin-parallel slip while the corresponding slabs subduct with slip normal to the margin. As a result, individual slivers of lithosphere (sliver plates) develop in the upper plate between the trench and its associated strike-slip faults (e.g. Fitch, 1972; Karig, 1978) (Fig. 1, panel A and B). These faults, reaching hundreds of kilometers of cumulative displacements along thousands of kilometers, favor localization of magmatic intrusions and influence the position of the volcanic arc (Sieh, 1988). Sense and rate of motion along these faults can be quantified using geophysical data, and large-scale domains of compression and tension can be identified in relation to the degree of convergent and divergent slip resulting from fault geometry (Prescott, 1981; Sieh, 1988).

The Peru-Chile trench and the Atacama fault in the west coast of South America (e.g. Allen, 1965), the Nankai Trough and the Median tectonic line in Japan (e.g. Kaneko, 1966), and the Sunda trench and the Sumatran Fault System in Sumatra Island (e.g. Katili, 1970; Fitch, 1972) are prominent examples of this particular tectonic setting highly prone to large, hazardous earthquakes. The system associated with the Sumatran Fault System (SFS) (Fig. 1.A) has attracted researchers, especially after the infamous 2004 Mw 9.1 earthquake off the west coast of northern Sumatra (Subarya et al., 2006; Fu and Sun, 2006; Chlieh et al., 2007; Franke et al., 2008). Intensive geophysical studies provide a good understanding of seismic coupling and vertical motions along the forearc side of the sliver plate (Simoes et al., 2004; Natawidjaja et al., 2004, 2006; Sieh, 2007; Berglar et al., 2010; Collings et al., 2012; Cook et al., 2014; Martin et al., 2014; Frederik et al., 2015). However, structural and kinematic analyses in the SFS and derived structures need to be improved to help evaluate the seismic hazard potential, and thus mitigate the impact of the devastating earthquakes associated with this system (e.g. Ishii et al., 2005; Moreno et al., 2010).

Sieh and Natawidjaja (2000) studied different sectors of the SFS using photo-interpretation in an area ranging from 6.75°S to 4.4°N; we study the geometry of the northern sector of Sumatra including the islands in northwest offshore Sumatra, which have not been described in detail in previous studies. Here, we investigate whether the structural framework of the northern sector of the Sumatran Fault System (NSFS) is variable,

and how this variability might reflect strain partitioning. To this end, we analyze new detailed structural data from the NSFS, with special attention to the aforementioned islands. These islands exhibit the youngest deformation in relation to oblique convergence, located at the leading edge of northwestwardly propagating continental sliver deformation exposed on land (Jarrard, 1986; McCaffrey, 1991, 1992).

2. Present day geodynamic context

2.1. Geometry, kinematics, volcanism and seismicity

The strike-slip SFS accommodates the high-angle oblique subduction of the Australian Plate below the Sunda Plate. The right-lateral transpressional SFS runs parallel to the trench with an overall linear, slightly sinusoidal geometry (e.g. Natawidjaja, 2002), and cuts the Sumatran lithosphere vertically down to the asthenosphere (Bellier and Sébrier, 1994). The SFS defines the eastern boundary of the Sumatran sliver plate; its western limit is the NNW-SSE curved Sunda Trench (Fitch, 1972; Karig, 1978; McCaffrey, 2009) (Fig. 1.A). This sliver plate thus represents an individualized sector of the Sunda Plate forearc (more than 1650 km long and 250-300 km wide), which moves northwestwards along the trench, driven by basal shear (McCaffrey et al., 2000; McCaffrey, 2009) (Fig. 1.B).

The Australian Plate moves northwards at a rate of 59 ± 3 mm·yr⁻¹ at the latitude of Sumatra Island, east of the Ninety East ridge; west of the ridge, the Indian Plate moves at a lower rate of 39 ± 3 mm·yr⁻¹ (Martin et al., 2014). Both, the Australian and Indian plates move almost parallel to the N-S trending Sunda Trench. The Sunda Trench shows pure dip slip motion at a mean rate of 45 mm·yr⁻¹, accommodating the normal-to-trench motion of Australia (Jarrard, 1986; McCaffrey, 1991, 1992; Bock et al., 2003). The movement parallel to the trench is partly ($\sim 2/3$) accommodated by strike-slip along the SFS at rate of 24.5 ± 4.5 mm·yr⁻¹ (Chlieh et al., 2008), and partly ($\sim 1/3$) by full margin parallel motion probably between the forearc islands and the trench (McCaffrey et al., 2000) (Fig. 1.A). Slip rates increase towards the northwest along the SFS, as indicated by the arcuate shape of the subduction trench, a distant pole of rotation, and earthquake slip vectors from the subduction mega-thrust, as well as GPS data (Huchon and LePichon, 1984; McCaffrey, 1991). Strain partitioning into dip-slip and strike-slip components is largest in northernmost Sumatra, due to the increasing obliquity between the orientation of the subduction trench and absolute plate motions.

101 The SFS transects Sumatra Island in its entirety and
 102 largely controls the tectonic architecture of the island
 103 (McCaffrey, 1991; Genrich et al., 2000; Simons et al.,
 104 1999; Bock et al., 2003; Socquet et al., 2006; Simons
 105 et al., 2007), which is prone to frequent volcanic eruptions
 106 and high magnitude earthquakes (e.g. Ninkovich
 107 et al., 1978; Walter and Amelung, 2007; Chlieh et al.,
 108 2008) (Fig. 1, panels C and D). The volcanic arc in
 109 Sumatra Island runs parallel to the subduction zone and
 110 sidewise with the SFS, above the 100-150 km depth
 111 contours of the subducting plate (Pesicek et al., 2008;
 112 Hatherton and Dickinson, 1969; Sieh and Natawidjaja,
 113 2000). The mechanically weaker behavior along the magmatic
 114 arc concentrates deformation and ultimately influences the
 115 position of the SFS, which in turn favors the location of
 116 volcanic centers within major releasing stepovers, while
 117 controlling the morphology of the volcanoes (Jarrard, 1986;
 118 McCaffrey, 1992; Bellier and Sébrier, 1994).

120 Locally, the SFS shows changes in strike resulting
 121 in tens of potentially-seismic fault defining releasing
 122 and restraining bends, that are several kilometers wide
 123 (Natawidjaja, 2002; Kasmolan et al., 2010). Such fault
 124 stepovers localize deformation and reduce the potential
 125 area of slip per seismic event. This leads to observed
 126 earthquake magnitudes of M_w 7.5 or smaller along the
 127 entire fault (McCaffrey, 1992). This local segmentation
 128 along the SFS leads to internal deformation in the
 129 forearc sliver plate (Katili and Hehuwat, 1967; Bellier
 130 and Sébrier, 1994; Prawirodirdjo et al., 2000; Sieh and
 131 Natawidjaja, 2000) (Fig. 1.D).

132 2.2. Geology of Northern Sumatra

133 Northwards of $\sim 5.05^\circ$ N, the SFS accommodates motion
 134 along two fault strands that diverge at an $\sim 30^\circ$ angle,
 135 creating two topographic highs and confining a topographic
 136 low in between (Fig. 2). For descriptive simplicity, we
 137 term these features as the eastern and western
 138 branches of the Northern sector of the Sumatran
 139 Fault System (NSFS) and the onshore basin, respectively.
 140 The motion along the branches of the NSFS readily
 141 controls the development of the topography bounding
 142 the onshore basin. Whereas the eastern branch transects
 143 basement igneous rocks and Miocene and Quaternary
 144 volcanic and sedimentary rocks, the western branch
 145 almost exclusively cuts basement igneous rocks
 146 (Fig. 2). This lithological contrast might be contributing
 147 to the different topographic heights between both
 148 branches; topography in the eastern branch of the NSFS
 149 is significantly lower than in the western branch, al-
 150 though the former encloses magmatic additions by at
 151 least two volcanic centers. The flat morphology of the

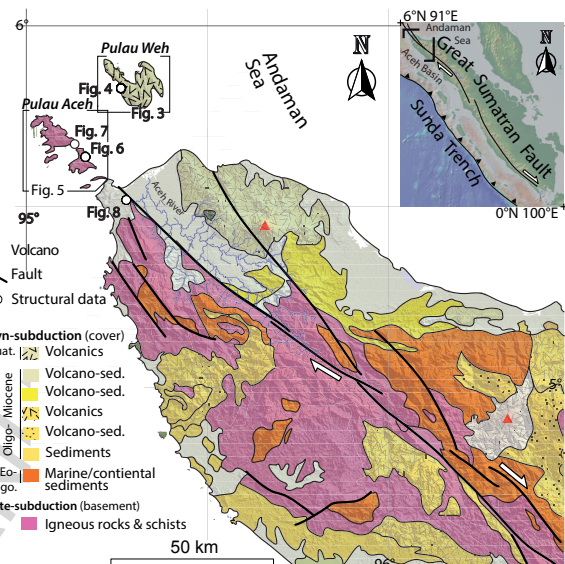


Figure 2. Simplified geologic map of the study area and surroundings (on top of the ASTER GDEM 1-arc), showing the main cover units (syn-subduction) on top of basement (ante-subduction). Location of the areas used during the DEM analyses, and that of the outcrops discussed in this contribution, and their corresponding figures, are also indicated.

152 onshore basin is controlled by the meandering dynamics
 153 of the Aceh river, flowing from the mountain highs in
 154 the south to the Andaman Sea, as the basin gains width,
 155 up to a maximum of ~ 35 km at the coast. Both fault
 156 branches run straight for at least ~ 80 km before reach-
 157 ing the northernmost coast of Sumatra, and continue far-
 158 ther northwest, running parallel to each other, off the
 159 coast of north Sumatra Island. Near the coast in the An-
 160 daman Sea, several islands develop in relation to each
 161 branch of the NSFS; the eastern branch runs through
 162 the Pulau Weh Island in the northernmost sector of the
 163 study area, while the western branch marks the eastern
 164 boundary of the Pulau Aceh archipelago in the western-
 165 most sector of the study area (Fig. 2). Farther north, the
 166 NSFS transforms into the Andaman spreading center at
 167 its northwestern terminus (Curry et al., 1979).

168 3. Structural analysis of Digital Elevation Models (DEMs) and in the field

170 We combined Digital Elevation Model (DEM) analy-
 171 sis and outcrop structural data in order to better define
 172 the geometry and kinematics of the NSFS. We per-
 173 formed structural interpretation of DEMs with a hori-
 174 zontal resolution of 30 m, derived from the Advanced

175 Spaceborne Thermal mission and Reflection Radiometer (ASTER GDEM) using the FaultTrace module of TerraMath WinGeol (TerraMath®). The FaultTrace tool uses the three point geometrical method of planar attributes in order to identify geological structures; the intersection line produced by the contact between topography and a geological planar feature (such as bedding or fault surfaces) is defined by at least three points, in turn characterizing the dip and dip direction of the geological object. To this end, the FaultTrace tool computes the best-fit plane defined by manually picked input points on the intersecting line. One relevant advantage of this tool is the ability to visually adjust the geological planes during mapping, thus constraining the most representative orientations. The error range is about $\sim 10^\circ$ for dip direction and $\sim 5^\circ$ for dip angle, thus slightly higher, but comparable to the uncertainties of field data acquisition (Reif et al., 2011). ASTER GDEM resolution is well suited for geometrical analysis of the topography to capture the main regional structures, but outcrop scale structures are not resolved. To produce better outcomes, we built our tectonic models focusing on the analysis of large-scale features and discarding numerous smaller, potentially ambiguous structures visible in the DEM. Similarly, to avoid confusion and map clustering, we have deliberately removed planar features that were observed too close to each other but provided the same information; in these cases, only the most representative, and often more pronounced, planar feature was plotted.

205 Additionally to our DEM analysis, we checked results in a field campaign with focus on outcrop-scale structural and kinematic analyses along the NSFS (Fig. 2). As no constraints on absolute timing of deformation exist for the area, we are only able to establish a relative chronology of deformation.

211 4. Geometry of the NSFS

212 We investigate the geometry of the NSFS at the northern end of Sumatra and at its northernmost offshore islands, i.e., between 4.5° N and 6° N latitude. We thus cover the fault from the location where it bifurcates as it propagates towards the northwest (Jarrard, 1986; McCaffrey, 1991, 1992), as well as the areas where the leading edge of deformation is exposed on land (Fig. 2 for location).

220 4.1. Pulau Weh Island and NSFS eastern branch

221 Pulau Weh Island is located in the northeast offshore prolongation of Sumatra Island at the eastern splay of

223 the NSFS (Fig. 2). Peninsulas trending NNW-SSE (i.e. parallel to the regional trend of the NSFS) control the shape of the Pulau Weh Island. Likewise, the first-order morphology of the island shows continuous topographic highs, indicating close relation to the NSFS. Our detailed topographic analysis reveals a minimum of eleven planar large-scale features (several kilometers in length) cutting the island (Fig. 3). These large-scale features can be bedding surfaces, faults or fractures. We classified these planar objects by analysing by their extension, shape, strike and dip, and pooled them into distinct sets. At least three different predominant sets of large-scale

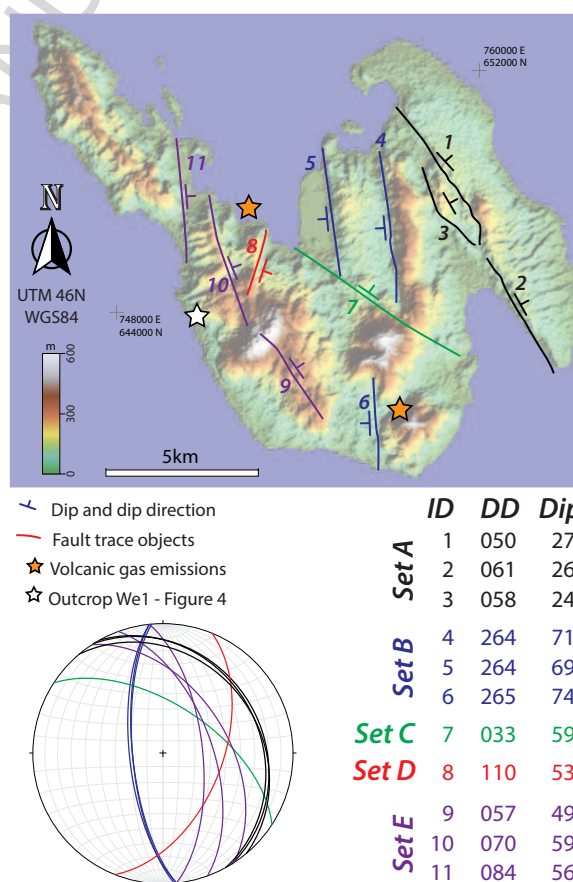


Figure 3. GDEM analysis of the Pulau Weh Island. On the left hand side is the topographic map of Pulau Weh and the structural features mapped with the FaultTrace module of TerraMath WinGeol (TerraMath®). Dip azimuth and dip angle are represented in map view and their values shown in table form, in the top right of the figure. Stereonet representation of such features is at the bottom right. Colours indicate different sets. A white star indicates the location of the Outcrop We1 (Fig. 4). Orange stars are used to locate areas with gas emission in relation to volcanic activity.

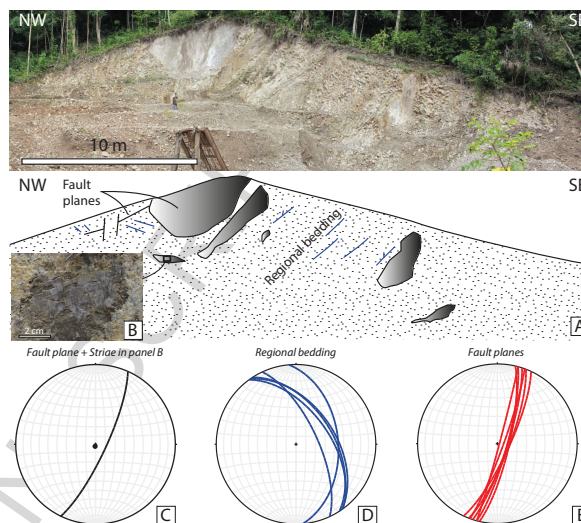
235 structures can be distinguished on the basis of strike and
 236 dip (Fig. 3). Lateral continuation and predominant oc-
 237 currence of planar features, marking most of the mor-
 238 phological highs in the island, suggest that these sets
 239 are related to faults rather than bedding.

240 A first set of large structures observed in the east-
 241 ern part of the island follows the main direction of the
 242 NSFS. Determined dip directions are constant towards
 243 the northeast with values of approximately 25° (Set A,
 244 black great circles in Fig. 3). The second cluster con-
 245 tains regional features that dip towards the west at an-
 246 gles of $\sim 70\text{--}75^\circ$ (Set B, blue great circles in Fig. 3). The
 247 maximum dip line of Set B is perpendicular to that of
 248 Set A. In the central region of the island, Set B bounds
 249 two pronounced ridges in the north and part of two topo-
 250 graphic highs in the south. Additionally, smaller struc-
 251 tures distributed across the entire island seem to fol-
 252 low the same trend. A third structure crosscuts the is-
 253 land in its central part, striking NW-SE, and dipping at
 254 $\sim 60^\circ$ towards the northeast (Set C, green great circle in
 255 Fig. 3). Farther west, a feature striking NNE-SSW, and
 256 dipping at $\sim 55^\circ$ towards the ESE, can be detected (Set
 257 D, Fig. 3, red great circle). Similarly to Set C, we note
 258 that the trend of Set D is observable across the entire
 259 island in local spots, but it is difficult to confidently in-
 260 terpret these smaller features. Finally, heading west, the
 261 strike direction of Set E resembles that of the NSFS in
 262 the south of the island and slightly rotates towards the
 263 NNE in its north. Similarly, dips progressively change
 264 from 50° to 65° towards the northwest (Set E, purple
 265 great circles, Fig. 3).

266 4.1.1. Outcrop We1 - $5^\circ 49' 39.92''\text{N}$; $95^\circ 15' 41.39''\text{E}$

267 Exposure, as well as access to most sectors of Pulau
 268 Weh Island, is very limited. However, at one spot at
 269 the central west coast, structures are well exposed at the
 270 scale of tens of meters, due to a relatively fresh road cut,
 271 allowing for multiple measurements of fault and bed-
 272 ding planes (Fig. 4).

273 A set of faults crosscuts the entire outcrop. Several
 274 fault planes are exposed, consistently dipping steeply
 275 towards the ESE. The single kinematic indicator found
 276 suggests top-to-the-southeast movement (Fig. 4). Bed-
 277 ding offset is not observed along this fault or any other,
 278 indicating that this normal component is not accommo-
 279 dating much strain. In the southeastern part of the out-
 280 crop, bedding surfaces constantly dip at an angle of ap-
 281 proximately 50° towards the northeast. Going farther to
 282 the northwest, beds dip at 70° towards SSE. The cross-
 283 cutting relationship between the two different plane sets
 284 is not exposed. However, the beds dipping $190/70$ form
 285 the southern limb of an upright similar fold, with its fold



286 Figure 4. Outcrop We1. A: Top image shows a panoramic picture of the
 287 outcrop, and its interpretation is at the bottom. Panel B is a close
 288 up of fault-related calcite and its striae. To the right, stereoplots of (C)
 289 the great circle for the fault plane and its striae in panel B, and great
 290 circles of (D) regional bedding (in blue) and of (E) main fault planes
 291 (in red).

292 axis plunging at 20° towards the west. This structure is
 293 cut by a fault dipping at 38° towards the northeast. No
 294 kinematic indicators were found on this fault.

295 4.2. Pulau Aceh Archipelago and NSFS western branch

296 Pulau Aceh is an archipelago composed of five
 297 curved-shaped islands located offshore northernmost
 298 Sumatra (Fig. 2), to the west of Pulau Weh Island. The
 299 eastern end of the Pulau Aceh Archipelago defines a
 300 sharp straight like trending NNW-SSE that coincides
 301 with the expected offshore prolongation of the western
 302 branch of the NSFS (Fig. 5).

303 The planar structures shown in Fig. 5 are the most
 304 prominent features, extending often along the entire is-
 305 lands in E-W direction. Based on their orientation, we
 306 distinguished three major sets of structures among a to-
 307 tal of 23 planar features (Fig. 5). Features of Set 1 strike
 308 ENE, have limited length (1-2 km along strike) and of-
 309 ten appear in clusters, with planes characterized by pe-
 310 riodic spacing (2 to 300 m). At archipelago scale, Set 1
 311 planes dip roughly north, and have dip values progres-
 312 sively increasing from subhorizontal to $\sim 50^\circ$ towards
 313 the south (Set 1, black great circles in Fig. 5). Set 2 con-
 314 sists of roughly S-dipping ENE-trending features that
 315 at occasions crosscut the whole length of the islands.
 316 Set 2 dip values progressively decrease southward, from
 317 45° to subhorizontal (Set 2, blue great circles in Fig. 5).

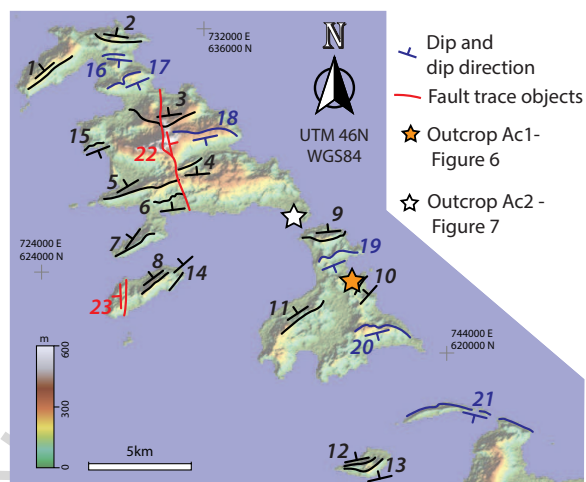
312 At the scale of the whole archipelago the strike of Set 1
 313 and Set 2 are similar, while their dips display a roughly
 314 constant angular relation of $\sim 45^\circ$. Set 3 is characterized
 315 by two opposite-dipping structures striking NNW with
 316 dip values of 60° that crosscut the two aforementioned
 317 planar sets of mappable structures (Set 3, red great circles,
 318 Fig. 5).

319 Structures in Set 1 are interpreted as regional bed-
 320 ding, given their limited lateral continuation, and peri-
 321 odical spatial distribution. Straight appearance and con-
 322 tinuity over many kilometers allow interpretation of Set
 323 2 and Set 3 as faults, shallow and steeply dipping, re-
 324 spectively. Heading to the southeast, dip values con-
 325 sistently increase for the regional bedding (Set 1) and
 326 decrease for the shallow dipping faults (Set 2), main-
 327 taining an angular relation of roughly 45° between both
 328 sets. This angular relation suggests that the shallow dip-
 329 ping faults affected consistently dipping regional beds.
 330 These faults were later rotated, reaching 45° at their
 331 northwest extent, leading in turn the variation in the
 332 bedding dips. Set 3 corresponds to younger steeply dip-
 333 ping fault planes crosscutting both the bedding and the
 334 shallow dipping fault set.

335 4.2.1. Outcrop Ac1 - $5^\circ 38' 17.10''N$; $95^\circ 09' 51.06''E$

336 Outcrop Ac1 is located in Pulau Nasi, one of the
 337 southern islands of Pulau Aceh Archipelago (Fig. 5 for
 338 location). Outcrop Ac1 reveals an almost complete 3D
 339 exposure of a stratigraphic sequence, transected by low
 340 angle reverse faults.

341 Outcrop Ac1 (Fig. 6) shows a shallowing upwards
 342 stratigraphic sequence. From bottom to top: (i) deep-
 343 water black shales, (ii) silt-shale alternations, and (iii)
 344 pluri-decametric channels filled with fluvial red sands
 345 and conglomerates. Northeastwards dipping regional
 346 bedding ($\sim 40^\circ$) is transected by faults dipping north
 347 from $\sim 40^\circ$ to $\sim 60^\circ$. The faults are located in the shales
 348 at the base the sequence and in the interlayered silt
 349 and shale levels. Often, fault planes filled with recrystal-
 350 lized cm-thick calcite are parallel or subparallel to bed-
 351 ding. A mesoscale fault-propagation-fold (tens of met-
 352 ers) is identified by the geometry of the transition from
 353 dark shales to lighter-colored silts in relation to a thrust
 354 plane (T1 in Fig. 6, panel A). Close to a W-E directed
 355 profile drawn by the topography, this stratigraphic con-
 356 tact hits the thrust plane at a low angle (upper left side
 357 of panel A). The same relation is observed on the other
 358 side of this three-dimensional exposure (a N-S directed
 359 profile), where this fault-bend fold is located above an-
 360 other thrust surface (T2 in Fig. 6 panel A and B).



	ID	DD	Dip		ID	DD	Dip	
Set 1	1	323	12	Set 2	16	183	46	
	2	013	27		17	154	13	
	3	352	26		18	168	22	
	4	356	23		19	159	12	
	5	334	13		20	164	11	
	6	350	14		21	190	01	
	7	303	07		Set 3	22	076	55
	8	329	05			23	273	60
	9	354	31					
	10	313	44					
	11	329	37					
	12	345	50					
	13	339	22					
	14	316	01					
	15	156	02					

Figure 5. GDEM analysis of the Pulau Aceh Archipelago. On the left hand side is the topographic map of the Pulau Aceh Archipelago and the structural features mapped with the FaultTrace module of TerraMath WinGeol (TerraMath®). Dip azimuth and dip angle are represented in map view and their values shown in table form, at the right hand of the figure. Stereoplot representation of such features is between the aforementioned panels. Colours indicate different sets of faults; beds are not shown. Orange and white stars indicate the location of the outcrop Ac1 and Ac2, respectively.

361 4.2.2. Outcrop Ac2 - $5^\circ 40' 12.77''N$; $95^\circ 07' 56.87''E$

362 Outcrop Ac2 is located in Pulau Breueh, one of the
 363 northern islands of Pulau Aceh Archipelago (Fig. 5 for
 364 location), and it exposes a deformed sedimentary series.

365 Outcrop Ac2 displays a series of interlayered sand-
 366 stones and siltstones affected by folds and faults. Re-
 367 gional bedding trend N50–N90°, dip 40° toward the
 368 SSE, and is often affected by low-amplitude folding.

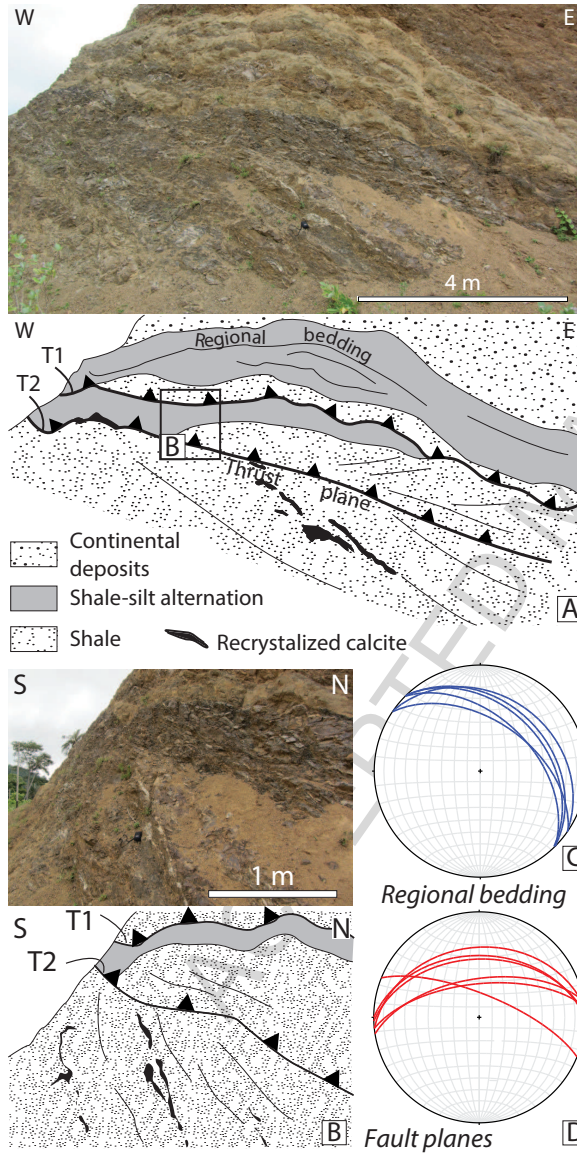


Figure 6. Outcrop Ac1. Panel A: Upper side shows a panoramic picture of the outcrop, with its interpretation below. Panel A is oriented roughly E-W, i.e. parallel to the thrust planes. Panel B: Close ups. Upper side shows calcite-filled veins parallel to the bedding, and below its schematic interpretation. Panel B is oriented roughly N-S, i.e. perpendicular to the thrust planes. Panel C and D: Stereoplots, with great circles for the regional bedding (in blue) and the shallow dipping faults (in red).

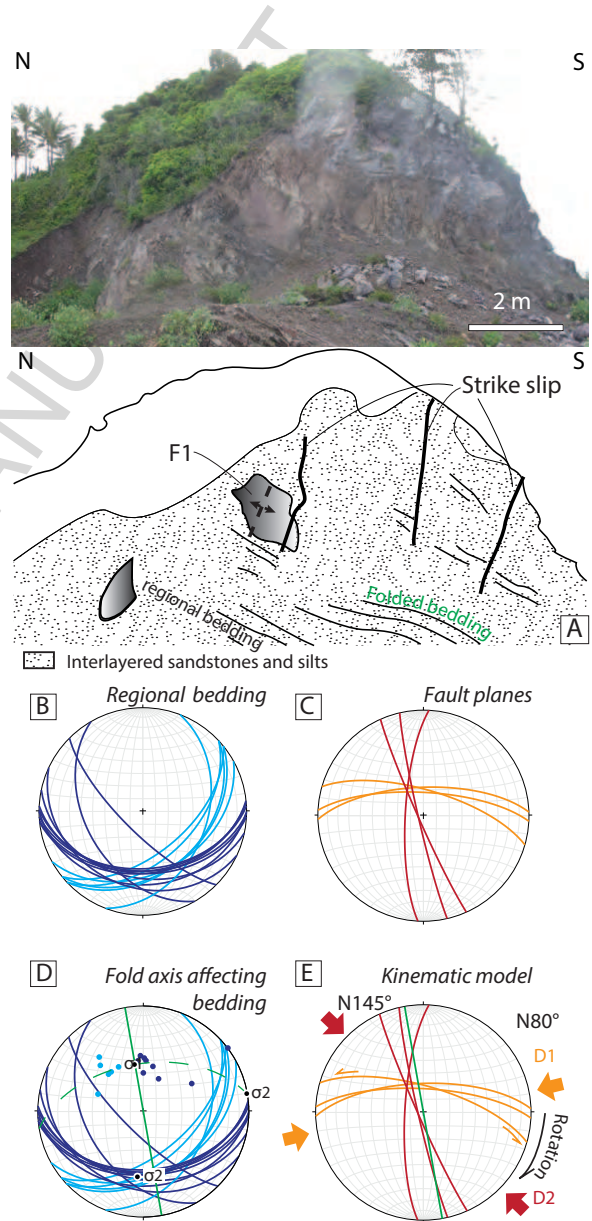


Figure 7. Outcrop Ac2. Panel A: Upper side shows a panoramic picture of the outcrop and below its interpretation. At bottom, stereoplots showing: [B] the great circles for the regional bedding (in two types of blue); [C] steeply dipping faults (in orange and red); [D] fold axial plane of the low-amplitude folds (in green); and [E] schematic kinematic model of stress field rotation.

369 The axial plane of this folding is vertical and strikes
 370 NNW-SSE ([D] in Fig. 7). We identified two distinct
 371 sets of features that cross-cut bedding without obvious
 372 vertical displacement, both with subvertical dips; (i) one
 373 set trending N-S and dipping west ([C, red] in Fig. 7),
 374 and (ii) another set oriented E-W and dipping to the
 375 north ([C, orange] in Fig. 7). The E-W set represent
 376 fault planes in two locations in the outcrop, which are
 377 crosscut by the N-S striking system and gently folded
 378 (F1 in Fig. 7). This structural setting fits well in a strike-
 379 slip setting.

380 4.2.3. Outcrop Su1 - $5^{\circ}31'08.35''N$; $95^{\circ}16'34.41''E$

381 Outcrop Su1 is located on Sumatra mainland near
 382 the northern coast and exposes a large continuous fault
 383 plane trending roughly NW-SE. The fault outcrops in a
 384 quarry and is aligned with the Pulau Aceh Archipelago
 385 eastern boundary (Fig. 2 for location).

386 Outcrop Su1 exhibits an excellent exposure of the
 387 NSFS fault plane with numerous well-preserved kine-
 388 matic indicators (Fig. 8). The fault plane dominat-
 389 ing the outcrop, roughly spanning an area of $\sim 450\text{ m}^2$,
 390 trends ESE-WNW and consistently dips at 54° to the
 391 SSW. This fault has a dextral-normal sense of move-
 392 ment, as shown by numerous striae and calcite recrystalliza-
 393 tions with kinematic indications that systematically
 394 indicate top-to-the-W motion and oblique slip plunging
 395 at 40° (see Fig. 8). Around 30 m to the SE, another
 396 large fault plane is roughly oriented N-S and dips at
 397 $\sim 80^{\circ}$ towards the west. Between these two systems a
 398 series of steeply dipping faults with no apparent vertical
 399 displacement deform the rocks into a tectonic breccia.
 400 Bedding dips gently to the west at the southeastern side
 401 of the outcrop, and becomes vertical near the main fault
 402 plane.

403 5. Structure and kinematics of the NSFS.

404 5.1. Interpretation of the observations in the outcrops

405 We interpret the faults exposed in Outcrop We1, with
 406 very steep dip and lack of significant vertical offset, as a
 407 strike-slip fault system for two main reasons. The spac-
 408 ing among the fault planes is irregular and they often
 409 appear in tight clusters, without branching/coalescence
 410 among planes, and overall resembles a broad area of
 411 a strike-slip corridor, in opposition to a “domino-like
 412 normal fault system. Furthermore, besides the presence
 413 of just one kinematic indicator, we tentatively allocate
 414 Outcrop We1 in relation to either Set D or Set E of our
 415 DEM analysis. The former interpretation is based on
 416 the coincidence in trend between the outcrop and Set

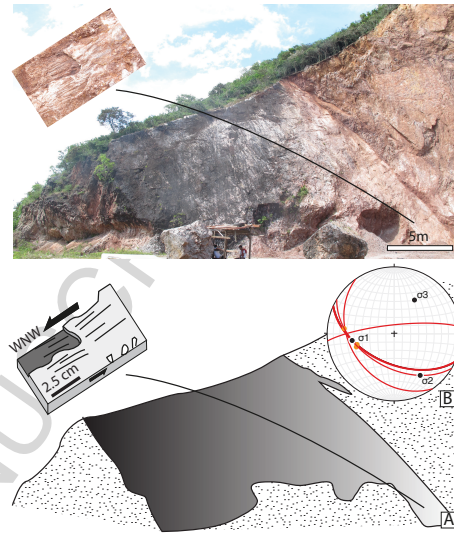


Figure 8. Outcrop Su1. Field picture [A] and its interpretation [B]. Inset shows a close up of the fault plane, with top-to-the-W strike-slip kinematic indicators. The stereonet shows several fault plane measurements and associated striae as well as the principal stress axes.

417 D. The latter interpretation is based on coincidence in
 418 location: Set E is geographically closer to the outcrop,
 419 which is in a southward position from Set E ID 11 and
 420 almost coincidental with its trend (if extrapolated lin-
 421 early south).

422 We interpret Outcrop Ac1 as the result of thrust ac-
 423 tivity. This interpretation can explain the shallowing-
 424 upwards stratigraphic sequence as the result of regional
 425 thrust-related uplift (leading to a tectonically induced
 426 regression), and the presence of the local thrusts and
 427 related folds that duplicate the stratigraphy. In the ab-
 428 sence of clearer kinematic indicators, i.e. striae, we in-
 429 fer northward thrust movement on the basis of the ge-
 430 ometry of the anticline at the hangingwall of T1 thrust
 431 plane. Strain is localized in the shale layers, where bed-
 432 ding parallel shear and calcite recrystallization is ob-
 433 served.

434 Outcrop Ac2 observations are symptomatic of strike-
 435 slip motion for the E-W set, even in the absence of
 436 kinematic indicators. Similarly, outcrop location and ir-
 437 regular distribution of the N-S striking set suggests an
 438 strike-slip origin, although the absence of a clear fault
 439 plane exposure cannot completely overrule their forma-
 440 tion as shear joints. From the orientation of fold axial
 441 planes we deduce an ENE-WSW trend for the princi-
 442 pal stress axis (σ_1). This ENE-WSW direction of σ_1
 443 is also compatible with a left lateral motion along the
 444 E-W strike-slip. We thus suggest that folding is coeval

445 with sinistral E-W strike-slip, and is the result of a single 495
 446 deformation event. Similarly, we consider that the 496
 447 uniform spatial distribution of tilted regional beds and 497
 448 their consistency with fold orientation are indicative of 498
 449 the development of both features as part of the afore- 499
 450 mentioned deformation event. Strain analysis based on 500
 451 assumed ideal stresses needed to develop the geometry 501
 452 of both features, when taken together suggests they de- 502
 453 veloped under an ENE-WSW σ_1 (D1, stereoplot [E], 503
 454 Fig. 7). Later, a second deformation event leads to the 504
 455 development of N-S strike-slip, transecting the previ- 505
 456 ously formed features, as inferred by the crosscutting 506
 457 relations (D2, stereoplot [E], Fig. 7). This later event 507
 458 suggests a clockwise rotation of the stress field from 508
 459 ENE-WSW to NW-SE ([E] in Fig. 7).

460 We interpret Outcrop Su1 as a large scale negative 510
 461 flower structure within the NSFS at this location. This 511
 462 interpretation is based on the dextral transtensive kin-
 463 matics of the dominating fault and the opposite dipping
 464 of the other major fault, taken together with the ap-
 465 parent lack of vertical displacement on the minor fault
 466 planes, and their orientation in coupling with the folding
 467 of bedding towards them. The overall configuration of
 468 Outcrop Su1 shows that strain may be distributed along
 469 the strike of the fault, and the damage zone related to
 470 the active fault may reach substantial widths. Further-
 471 more, this kinematic setting, despite fitting the overall
 472 framework, is different from the observations on Pulau
 473 Aceh and Pulau Weh islands. This differences indicate
 474 variability of kinematics of the NSFS within small dis-
 475 tances, and stresses the need for detailed analysis of the
 476 respective subsystems.

477 5.2. The Pulau Weh riedel system

478 The observed structures, taken together with the tec-
 479 tonic strike-slip framework of the Pulau Weh Island and
 480 its geographic location, atop of the eastern fault branch
 481 of the NSFS, allow us to interpret it as a Riedel sys-
 482 tem (Fig. 9). Indeed the strike directions of observed
 483 large-scale structures fit remarkably well with strike di-
 484 rections within a Riedel system. However, additional
 485 complexity is revealed when taking into account dip
 486 variations. Analysis of the different topographic fea-
 487 tures allows for pooling determined structures into dis-
 488 tinct sets of mappable structures. The most prominent
 489 set (Set A), which dominates the morphology of the en-
 490 tire island, is parallel to the NSFS. In a Riedel frame-
 491 work, it corresponds to the main direction of imposed
 492 shear, oriented at a 45° angle from the maximum com-
 493 pressive stress (Fig. 9). Set B, which is oriented at an
 494 angle of approximately 15° to the direction of Set A

correlates to R-shears, while Set C corresponds to P-
 shears. Even though R-shears are not apparent in our
 DEM analysis, several small scale features, especially in
 the southernmost part of the island, could be interpreted
 as such. We note that Set E changes strike and dip di-
 rection from east to west. We interpret this as a local
 particularity, i.e. as variations within the main direc-
 tion of fault strike with respect to σ_1 . Our outcrop anal-
 ysis on Sumatra Island showed that such variations can
 be reasonably expected within the overall framework.
 This is corroborated by complex topography and high-
 est peaks on the island, which may be the result of a
 positive flower structure in this area. Consequently, we
 interpret Set D as R-Shears with respect to Set E. Like-
 wise outcrop We1 fits in the overall Riedel system, and
 corresponds to local variation of Set E, that is the main
 direction of imposed shear.

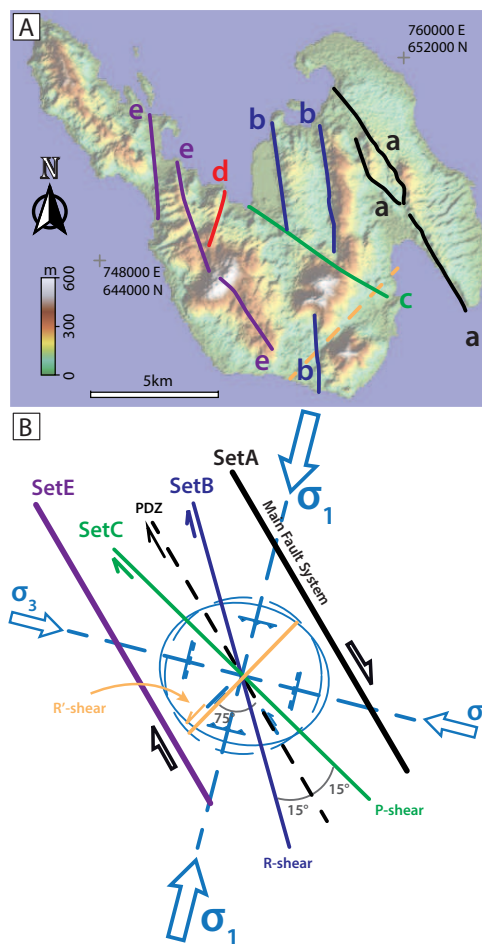


Figure 9. Structural interpretation in Pulau Weh: Riedel system.

Dip of the respective systems and limited knowledge on their kinematics complicate this straightforward interpretation. Particularly, due to the inclined nature of the faults, the 45° between inferred maximum compressive stress and strike of the shear zone, as interpreted from map view (Fig. 9), may be smaller in reality. Moreover, set C could likewise be seen as thrust faults in the overall transpressive framework, in turn fitting our interpretation of local flower structures in other areas. Most surprising are the rather shallow dips of Set A in the eastern part of the island. Judging from their dip only suggests thrust fault kinematics of the faults. It remains difficult to determine whether these structures initiated as thrust faults and were later reactivated with strike-slip kinematics, or initial strike-slip structures have been rotated. A potential driver for thrust faulting might be push of the Australian Plate. However, if the structures initiated as thrust faults, this would require later rotation of the stress field in such a way that the orientation of the NSFS perfectly coincides with orientation of the thrust faults of the compressive regime (i.e. rotation of σ_1 by 45°). Even though this cannot be excluded, we prefer the interpretation of later rotation of the faults and their formation within the Riedel framework. A first order test for the different hypotheses that may be carried out in the future would contain detailed field mapping of cross cutting relationships of kinematic indicators on the fault planes. In sum, we argue that the overall structural configuration of Pulau Weh Island fits within a Riedel framework, but shows partly significant complexity and deviations from a simple pattern. This potentially provides additional insights on how the strike-slip faults evolve during northwestward propagation.

The existence of Pulau Weh Island begs the question as to its cause. Within the strike-slip environment, and most importantly due to its northwestward propagation, significant amount of uplift within the sliver plate may be expected, first due to frontal and basal accretion, and secondly due to positive flower structures. Such vertical extrusion can lead to significant amount of topography, as for instance observed in the Eastern California Shear Zone (e.g. Unruh et al., 2003). As the morphology of the island is largely dominated by faults, volcanic uplift may be considered subordinate at first sight. However, the topography onshore northeast Sumatra, which is similarly fault-controlled, is clearly dominated by the Seulawah Agam active volcano. Moreover, as large-scale strike-slip faults influence the location of the volcanic arc, it cannot be excluded that at least part of the uplift is related to volcanic activity. Indeed volcanic gas emissions occur on the island (orange stars in Fig. 3).

We suspect that at least partly the observed structural complexity may be caused by underlying volcanoes, as has been discussed for other areas. For instance the South Iceland Seismic Zone is a strike-slip zone that developed in close relation to the Icelandic Mantle Plume. Here, transform faulting of a relatively thin brittle layer above a hot viscous domain results in elastic response to deformation and rotation of relatively rigid blocks (Angelier et al., 2008). Another prominent example of strain partitioning and strike-slip motion within a magmatic arc is the southern Andes. Here, fault kinematic analysis shows that partly volcanoes are not structurally linked to adjacent strike-slip faults, but overall volcanic dikes and their root zones are associated with strike-slip structures such as horsetails or splays, reflecting the large scale stress field (Rosenau et al., 2006). Based on DEM analyses, the total amount of volcanic extrusion in the area has been quantified to range between 10 and 13 km³/km/Ma (Völker et al., 2011). For Sumatra, the coincidence between volcanic activity and location of the SFS has been recognized and described in several studies (e.g. McCaffrey et al., 2000; McCaffrey et al., 2001; Acocella, 2014). However, as to what extend magmatic activity controls structural evolution of the SFS or vice versa remains unclear, as where in some areas the fault and volcanoes coincide, in other parts strain localization is independent of volcanic activity (Genrich et al., 2000). Our detailed analysis may provide some insights, even though untangling the ultimate cause of uplift of Pulau Weh is difficult based on our data set. The large-scale structural pattern of the island seems to reflect strike-slip movements. However, the multiple local complexities do not fit this overall pattern, which suggests volcanic activity instead. Even though the role of volcanic activity leading to strain localization should not be underestimated, the tangled interaction between volcanic activity, stress and finite strain requires exhaustive analysis and mapping (Feuillet et al., 2006; Feuillet, 2013).

5.3. The Pulau Aceh thrust splays

As opposed to Pulau Weh Island, the Pulau Aceh Archipelago does not show such a distinct Riedel pattern. Instead, the character, dip direction and dip of the planar features mapped in the archipelago let us to the interpretation of the archipelago as a train of anticlines with opening angles of consistently $\sim 45^\circ$ (Fig. 10). Such fold trains may occur in the vicinity of strike-slip zones, especially when shallow weak layers facilitate detaching of the overlying strata (e.g. Twiss and Moores, 1992)(Figs. 10 and 11). Fold trains evolve

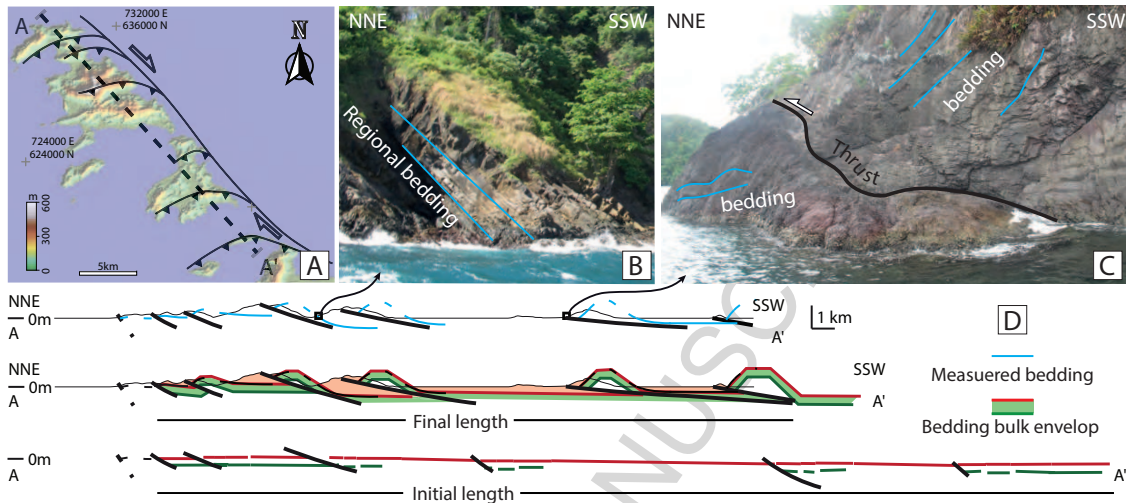


Figure 10. Structural interpretation of the Pulau Aceh: Fold-and-thrust splays.

614 in such hybrid situations as splay contractional structures of the overall strike-slip system. The anticlines
 615 show a systematic southward decrease of the angle of their basal fault. The southernmost fault dips at an
 616 angle of 30° , which is the typical angle for newly established thrust faults. Consequently we speculate that
 617 the northern fault has been rotated at a later stage, indicating southward out-of-sequence propagation of
 618 the thrusts. Such break-back sequences are common, and have been reported from various fold-and-thrust
 619 belts, for instance the European Alps (von Hagke et al., 2014b). It is noteworthy, that such fold-and-thrust
 620 belts are perpendicular to the fold-and-thrust belts, which form at the distal part of the sliver plate. This frame-
 621 work however requires the existence of a weak horizon within the involved sedimentary sequence, as well
 622 as predominance of the strike-slip component in the area. Such weak horizon may correspond either to the
 623 basement-cover interface or some rheological heterogeneities within the sedimentary sequence, such as the
 624 presence of deep marine shales, which are well-known décollement horizons (e.g. Rutter et al., 2013; Aydin
 625 and Engelder, 2014; Suppe, 2014). It has been shown that fluid overpressure may be an important factor; how-
 626 ever it is not necessary for producing extremely weak shale décollement (von Hagke et al., 2014a; Morley
 627 et al., 2014). Likewise, mineralogy, amount of organic matter or structure localisation may play an important
 628 role (e.g. Rutter et al., 2013).

643 5.3.1. Shortening in the contractional domain

644 To estimate the shortening in the fold-and-thrust system of Pulau Weh, we extrapolated the bedding bulk
 645 envelop from measurements taken in outcrops, and the planar structures extracted from the DEM. Based on this
 646 bulk envelop of the bedding, we performed a restoration. As the ages of the geological formations remain
 647 poorly constrained, this restoration is only based on the geometry of the contractional system. Note that
 648 this restoration is spatially limited as we restore the deformation along the last 30 km of the NSFS. The
 649 final section length is 40 km after unfolding of the bedding. Therefore, the amount of shortening accom-
 650 modated by the fold-and-thrust system in this area is ~ 10 km. This cross-section restoration through Pulau
 651 Aceh Archipelago allows us to give a tentative minimum shortening of 20% for the area (Fig. 10).

660 The geometry of the thrust splay suggests that the thrust faults root on a décollement layer at shallow
 661 depth. As 20% of deformation is accommodated in the fold-and-thrust belt, layer parallel shearing on this
 662 décollement is an important player in the overall strike-slip setting. This may be a relative important finding, as
 663 thrust systems are more likely to cause tsunami waves as opposed to strike-slip settings, which have limited
 664 tsunami hazard (Hornbach et al., 2010). Consequently quantifying the total amount of slip deficit on these
 665 structures may contribute to geohazard assessment of the area.

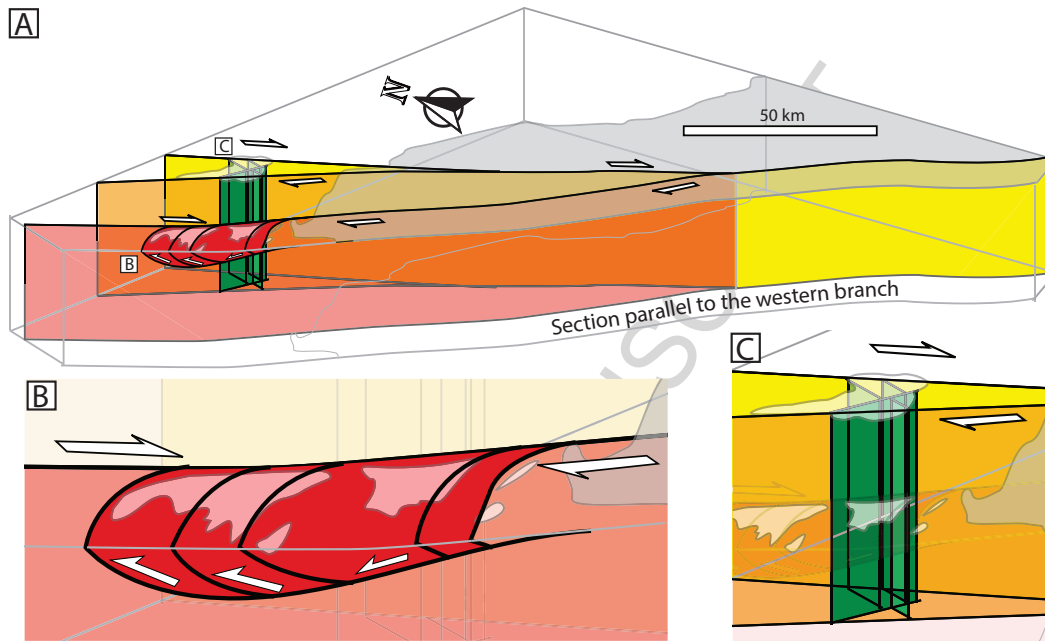


Figure 11. 3D kinematic model for the NSFS, representing the main structures and their motion in a view parallel to its western branch. Close-up view of the fold-and-thrust system in the western branch [B] and the Riedel system in the eastern branch [C].

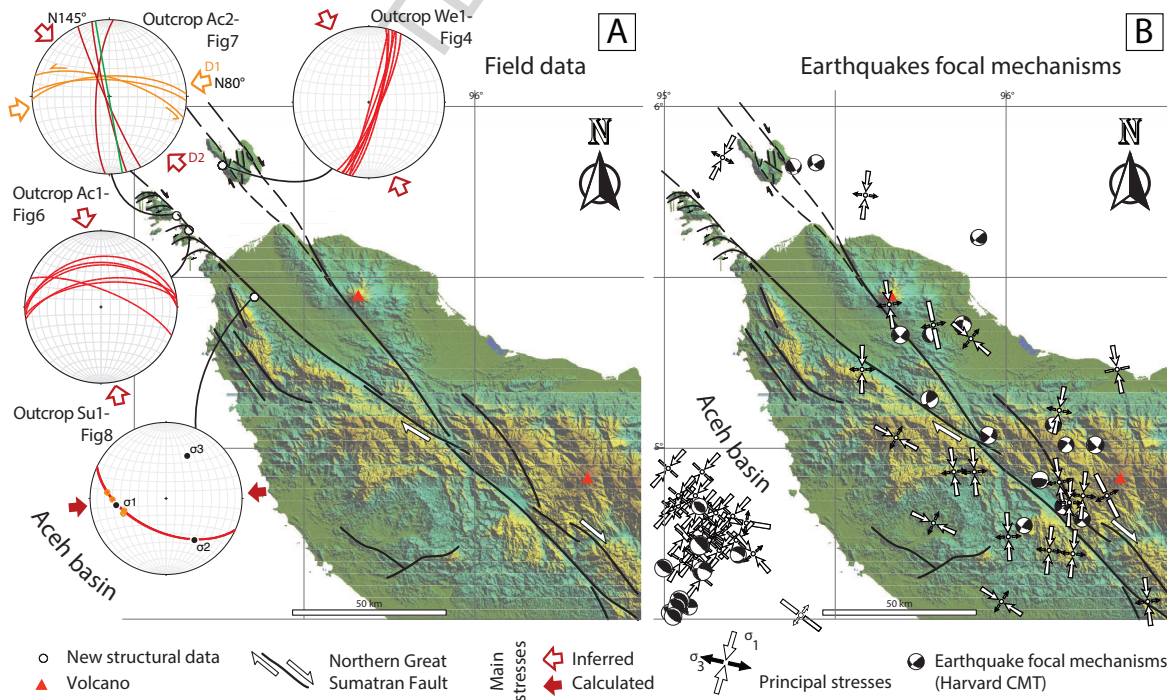


Figure 12. A: Stereoplots showing the analysis of structural data in few selected outcrops. B: Focal mechanisms derived from earthquakes, plotted with FSA software (Célérier, 2011).

5.4. Stress and strain in the NSFS

Here we show that a Riedel system trending NNW-SSE and a NW-verging thrust splay system developed to the East and West of the NSFS, respectively (Figs. 11 and 12). These strain patterns were both developed under a stress field characterized by a σ_1 and σ_3 roughly trending NNE-SSW and ESE-WNW, respectively (Fernández-Blanco et al., 2015). These directions are similar to the present day principal stress axes (e.g. McCaffrey, 2009) (Figs. 12). This observation suggests a stable stress field over a certain time period that remains difficult to estimate, since the stratigraphy is poorly constrained in the area, and therefore hinders a detailed chronology of both, deposits and deformation.

Observations of the Aceh Basin suggest that the NW-verging thrust splay system of the NSFS may be a lateral step over, connecting two strike-slip fault segments that will be eventually cross-cut as the NSFS farther propagates (Berglar et al., 2010; Martin et al., 2014). Strain seems to be accommodated at present day west off Sumatra mainland, along a strike-slip fault system bounding the West of the Aceh Basin and trending parallel to the NSFS, the West Andaman Fault (WAF) (Berglar et al., 2010; Martin et al., 2014) (Fig. 1). Berglar et al. (2010) propose that the WAF has been active since the Late Miocene, and propagates northwardly due to oblique convergence. South of the Aceh Basin, a series of thrust faults consist in a lateral step over connecting two strike-slip faults. These faults are similar to the one we described onshore. Additionally, Martin et al. (2014) show that the WAF cross cuts former thrust faults that have initiated a the tip of a propagating strike-slip fault. Therefore, we consider possible that a similar system is developing in the NSFS area.

Moreover, mechanical models show that the tips of large-scale propagating faults develop an tensional and a compressional damage zone (e.g. Hubert-Ferrari et al., 2003). This principle was applied to explain the evolution of the Aegean as the result of the combined effect of its backarc extension in relation rollback of the Hellenic slab towards Africa (Brun and Faccenna, 2008) and the compressional damage zone developed to the south of the propagating tip of the North Anatolian Fault (Armijo et al., 2003). Similarly, our observations of the tip of the NSFS match this stress pattern, with a western compressional domain (Pulau Weh thrust splay) and an eastern tensional domain (Pulau Aceh riedel system). However, whereas the stress pattern of the Aegean results from both fault propagation mechanics and backarc extension by rollback, the Sunda slab is not rolling back, and thus the Sumatran backarc region is only influenced by extrusion of SE Asia in response to India-Eurasia collision

(Peltzer and Taponnier, 1988). For the first time, we imaged the strain partitioning resulting from the propagation of the NSFS in Sumatra mainland (Fig. 11).

6. Conclusions

In this study we provided detailed structural analysis of the leading edge of deformation of the Sumatran Fault System, where strain is partitioned along two major fault branches. Our analysis reveals that kinematics at the exposed tip of the continental sliver features very different kinematic regimes within a relatively small area. For instance, in case of the Pulau Weh Island at the eastern branch of the NSFS, the overall structural pattern in map view represents a Riedel system. However, detailed analysis of dips of the planes in combination with uncertainty of their kinematics reveals that at least locally this big structure features complex areas, potentially related to late stage rotation of the strike-slip faults, flower structures, or transpressive thrust faults. Probably the most exciting finding of this study is the existence of a fold-and-thrust belt oriented perpendicular to the main strike direction of the large-scale strike-slip system. This secondary fold-and-thrust belt requires the existence of a weak décollement within the involved stratigraphic sequence. Importance of such weak décollement has been widely recognized in compressional settings. This study shows that they may evolve and significantly contribute to strain accommodation also in strike-slip settings, potentially related to the early stages of system evolution. This has major implications for geohazard assessment within the area; even though there are examples of strike-slip events causing tsunami (Hornbach et al., 2010), thrust faults are more likely to trigger tsunami. This study emphasizes that, in addition to GPS-based neotectonic and geophysical studies, field evidence is an essential requirement.

7. Acknowledgments

The authors want to thank the insightful comments and valuable input of the reviewers Sean Gulick and Juan Carlos Balanyá Roure, and to the editor, Manuel Díaz-Azpiroz. Wolfgang Straka and the project “Animal Perception of Seismic and Non-Seismic Earthquake Phenomena”, funded by Red Bull Media House GmbH, made this contribution possible. D. Fernández-Blanco is indebted with Awaluddin Yusuf, Syehaffer Wahyudi, Teuku Reza and Lono Satrio for their effort on the fieldwork logistics and enjoyable company.

771 **References**

- 772 Acocella, V., 2014. Structural control on magmatism along divergent and convergent plate boundaries: Overview, model, problems. *Earth-Science Reviews* 136, 226–288.
- 773 Allen, C., 1965. Transcurrent faults in continental areas. *Royal Society of London Philosophical Transactions* 258, 8289.
- 774 Angelier, J., Bergerat, F., Stefansson, R., Bellou, M., 2008. Seismotectonics of a newly formed transform zone near a hotspot: Earthquake mechanisms and regional stress in the South Iceland Seismic Zone. *Tectonophysics* 447, 95–116.
- 775 Armijo, R., Flerit, F., King, G., Meyer, B., 2003. Linear elastic fracture mechanics explains the past and present evolution of the Aegean. *Earth and Planetary Science Letters* 217, 85–95.
- 776 Aydin, M.G., Engelder, T., 2014. Revisiting the Hubbert–Rubey pore pressure model for overthrust faulting: Inferences from bedding-parallel detachment surfaces within Middle Devonian gas shale, the Appalachian Basin, USA. *Journal of Structural Geology* 69, 519–537.
- 777 Bellier, O., Sébrier, M., 1994. Relationship between tectonism and volcanism along the Great Sumatran Fault Zone deduced by SPOT image analyses. *Tectonophysics* 233, 215–231.
- 778 Berglar, K., Gaedicke, C., Franke, D., Ladage, S., Klingelhoefer, F., Djajidihardja, Y., 2010. Structural evolution and strike-slip tectonics off north-western Sumatra. *Tectonophysics* 480, 119132.
- 779 Bock, Y., Prawirodirdjo, L., Genrich, J.F., Stevens, C.W., McCaffrey, R., Subarya, C., Puntodewo, S.S.O., Calais, E., 2003. Crustal motion in Indonesia from Global Positioning System measurements. *Journal of Geophysical Research* 108(B8), 2367.
- 780 Brun, J., Faccenna, C., 2008. Exhumation of high-pressure rocks driven by slab rollback. *Earth and Planetary Science Letters* 272, 1–7.
- 781 Célérier, B., 2011. FSA: Fault and Stress Analysis Software, version 33.8. Univ. Montpellier 2.
- 782 Chlieh, M., Avouac, J.P., Hjorleifsdottir, V., Song, T.R.A., Ji, C., Sieh, K., Sladen, A., Hebert, H., Prawirodirdjo, L., Bock, Y., et al., 2007. Coseismic slip and afterslip of the great Mw 9.15 Sumatra–Andaman earthquake of 2004. *Bulletin of the Seismological Society of America* 97, S152–S173.
- 783 Chlieh, M., Avouac, J.P., Sieh, K., Natawidjaja, D., Galetzka, J., 2008. Heterogeneous coupling of the Sumatran megathrust constrained by geodetic and paleogeodetic measurements. *Journal of Geophysical Research* 113, B05305.
- 784 Collings, R., Lange, D., Rietbrock, A. and Tilmann, F., Natawidjaja, D., Suwargadi, B., Miller, M., Saul, J., 2012. Structure and seismogenic properties of the Mentawai segment of the Sumatra subduction zone revealed by local earthquake traveltimes tomography. *Journal of Geophysical Research* 117, B01312.
- 785 Cook, B.J., Henstock, T.J., McNeill, L.C., Bull, J.M., 2014. Controls on spatial and temporal evolution of prism faulting and relationships to plate boundary slip offshore north-central Sumatra. *Journal of Geophysical Research: Solid Earth* 119, 5594–5612.
- 786 Curray, J., Moore, D., Lawver, L., Emmel, F., Raitt, R., Henry, M., Kieckhefer, R., 1979. Tectonics of the Andaman Sea and Burma: Convergent margins. *American Association of Petroleum Geologists Bulletin*.
- 787 Fernández-Blanco, D., Philippon, M., von Hagke, C., 2015. Present-day stress orientations in the Great Sumatran Fault in North Sumatra. *Geotectonic Research* 97, 30–33.
- 788 Feuillet, N., 2013. The 2011/2012 unrest at Santorini rift: Stress interaction between active faulting and volcanism. *Geophysical research letters* 40, 3532–3537.
- 789 Feuillet, N., Coco, M., Musumeci, C., Nostro, C., 2006. Stress interaction between seismic and volcanic activity at Mt Etna. *Geophysical journal international* 164, 697718.
- 790 Fitch, T., 1972. Plate convergence, transcurrent faults, and internal deformation adjacent to Southeast Asia and the western Pacific. *Journal of Geophysical Research* 77, 44324460.
- 791 Franke, D., Schnabel, M., Ladage, S., Tappin, D.R., Neben, S., Djajidihardja, Y.S., Müller, C., Kopp, H., Gaedicke, C., 2008. The great Sumatra–Andaman earthquakes imaging the boundary between the ruptures of the great 2004 and 2005 earthquakes. *Earth and Planetary Science Letters* 269, 118–130.
- 792 Frederik, M.G.C., Gulick, S.P.S., Austin, J.A., Bangs, N.L., Udrek, 2015. Investigation of accretionary wedge structures off north Sumatra using 2D multichannel seismic and multibeam bathymetric data. *Tectonics* 34. doi:10.1002/2014TC003614.
- 793 Fu, G., Sun, W., 2006. Global co-seismic displacements caused by the 2004 Sumatra–Andaman earthquake (Mw 9.1). *Earth, planets and space* 58, 149–152.
- 794 Genrich, J., Bock, Y., McCaffrey, R., Prawirodirdjo, L., Stevens, C., Puntodewo, S., Subarya, C., Wdowinski, S., 2000. Distribution of slip at the northern Sumatran fault system. *Journal of Geophysical Research* 105, B12, 28,327–28,341.
- 795 Gudmundsson, Ó., Sambridge, M., 1998. A regionalized upper mantle (rum) seismic model. *Journal of Geophysical Research: Solid Earth* 103, 7121–7136.
- 796 von Hagke, C., Oncken, O., Evseev, S., 2014a. Critical taper analysis reveals lithological control of variations in detachment strength: An analysis of the Alpine basal detachment (Swiss Alps). *Geochimistry, Geophysics, Geosystems* 15, 176–191.
- 797 von Hagke, C., Oncken, O., Ortner, H., Cederbom, C., Aichholzer, S., 2014b. Late Miocene to present deformation and erosion of the Central Alps Evidence for steady state mountain building from thermokinematic data. *Tectonophysics* 632, 250–260.
- 798 Hatherton, T., Dickinson, W.R., 1969. The relationship between andesitic volcanism and seismicity in Indonesia, the Lesser Antilles, and other island arcs. *Journal of Geophysical Research* 74, 530110.
- 799 Heuret, A., Lallemand, S., 2005. Plate motions, slab dynamics and back-arc deformation. *Physics of the Earth and Planetary Interiors* 149, 31–51.
- 800 Hornbach, M.J., Braudy, N., Briggs, R.W., Cormier, M.H., Davis, M.B., Diebold, J.B., Dieudonne, N., Douilly, R., Frohlich, C., Gulick, S.P., et al., 2010. High tsunami frequency as a result of combined strike-slip faulting and coastal landslides. *Nature Geoscience* 3, 783–788.
- 801 Hubert-Ferrari, A., King, G., Manighetti, I., Armijo, R., Meyer, B., Tapponnier, P., 2003. Long-term elasticity in the continental lithosphere: modelling the aden ridge propagation and the anatolian extrusion process. *Geophysical Journal International* 153, 111–132.
- 802 Huchon, P., LePichon, X., 1984. Sunda Strait and central Sumatra fault. *Geology* 12, 668672.
- 803 Ishii, M., Shearer, P.M., Houston, H., Vidale, J.E., 2005. Extent, duration and speed of the 2004 Sumatra–Andaman earthquake imaged by the Hi-Net array. *Nature* 435, 933–936.
- 804 Jarrard, R., 1986. Terrain motion by strike-slip faulting of fore arc slivers. *Geology* 14, 780783.
- 805 Kaneko, S., 1966. Transcurrent displacement along the median line, south-western Japan. *New Zealand Journal of Geology and Geophysics* 2, 45–59.
- 806 Karig, D.E., 1978. Material transport within accretionary prisms and the “knocker” problem. *The Journal of Geology* 88, 2739.
- 807 Kasmolan, M., Santosa, B.J., Lees, J.M., Utama, W., 2010. Earthquake source parameters at the sumatran fault zone: Identification of the activated fault plane. *Central European Journal of Geosciences* 2, 455–474.
- 808 Katili, J., 1970. Large transcurrent faults in southeast Asia with spherical reference to Indonesia. *Geol. Rundsch.* 59, 581600.
- 809 Katili, J., Hehuwat, F., 1967. On the occurrence of large transcurrent faults in Sumatra, Indonesia. *Osaka University Journal of Geo-*

- science 10, 5–17.
- 901 Martin, K.M., Gulick, S.P., Austin, J.A., Berglar, K., Franke, D.,
902 2014. The West Andaman Fault: a complex strain-partitioning
903 boundary at the seaward edge of the Aceh Basin, offshore Suma-
904 tra. *Tectonics* 33, 786–806.
- 905 McCaffrey, R., Wark, D., Roecker, S., Ibrahim, G., et al., 2001. Distri-
906 bution of magma beneath the Toba caldera complex, north Suma-
907 tra, Indonesia, constrained by three-dimensional P wave velocities,
908 seismicity, and gravity data. *Geochemistry, Geophysics, Geosys-*
909 *tems* 2.
- 910 McCaffrey, R., 1991. Slip vectors and stretching of the Sumatran fore
911 arc. *Geology* 19, 881–884.
- 912 McCaffrey, R., 1992. Oblique plate convergence, slip vectors,
913 and fore arc deformation. *Journal of Geophysical Research* 97,
914 89058915.
- 915 McCaffrey, R., 2009. The tectonic framework of the Sumatran subduc-
916 tion zone. *Annual Review of Earth and Planetary Sciences* 37,
917 345–366.
- 918 McCaffrey, R., Zwick, P.C., Bock, Y., Prawirodirdjo, L., Genrich, J.F.,
919 Stevens, C.W., Puntodewo, S., Subarya, C., 2000. Strain partition-
920 ing during oblique plate convergence in northern Sumatra: Geode-
921 tic and seismologic constraints and numerical modeling. *Journal*
922 *of Geophysical Research* 105, 28363–28.
- 923 Moreno, M., Rosenau, M., Oncken, O., 2010. 2010 Maule earth-
924 quake slip correlates with pre-seismic locking of Andean subduc-
925 tion zone. *Nature* 467, 198–202.
- 926 Morley, C.K., Warren, J., Tingay, M., Boonyasaknanon, P., Julapour,
927 A., 2014. Comparison of modern fluid distribution, pressure and
928 flow in sediments associated with anticlines growing in deepwater
929 (Brunei) and continental environments (Iran). *Marine and*
930 *petroleum geology* 55, 230–249.
- 931 Natawidjaja, D., Sieh, K., Chlieh, M., Galetzka, J., Suwargadi, B.,
932 Cheng, H., Edwards, R., Avouac, J.P., Ward, S., 2006. Source
933 parameters of the great Sumatran megathrust earthquakes of 1797
934 and 1833 inferred from coral microatolls. *Journal of Geophysical*
935 *Research* 111, B06403.
- 936 Natawidjaja, D., Sieh, K., Ward, S., Cheng, H., Edwards, R., Galet-
937 zka, J., Suwargadi, B., 2004. Paleogeodetic records of seismic and
938 aseismic subduction from central Sumatran microatolls, Indonesia.
939 *Journal of Geophysical Research* 109, B04306.
- 940 Natawidjaja, D.H., 2002. Neotectonics of the Sumatran Fault and
941 paleogeodesy of the Sumatran subduction zone. Ph.D. thesis. Cal-
942 ifornia Institute of Technology.
- 943 Ninkovich, D., Sparks, R., Ledbetter, M., 1978. The exceptional mag-
944 nitude and intensity of the Toba eruption, Sumatra: an example of
945 the use of deep-sea tephra layers as a geological tool. *Bulletin*
946 *Volcanologique* 41, 286–298.
- 947 Peltzer, G., Taponnier, P., 1988. Formation and evolution of strike-slip
948 faults, rifts, and basins during the India-Asia Collision: An experi-
949 mental approach. *Journal of Geophysical Research* 93, 15085–
950 15117.
- 951 Pesicek, J., Thurber, C., Widiyantoro, S., Engdahl, E., DeShon, H.,
952 2008. Complex slab subduction beneath northern Sumatra. *Geo-*
953 *physical Research Letters* 35, L20303.
- 954 Prawirodirdjo, L., Bock, Y., Genrich, J., Puntodewo, S., Rais, J., Sub-
955 ariya, C., Sutisna, S., 2000. One century of tectonic deformation
956 along the Sumatran fault from triangulation and Global Posi-
957 tioning System surveys. *Journal of Geophysical Research* 105,
958 28,34328,363.
- 959 Prescott, W.H., 1981. The determination of displacement fields from
960 geodetic data along a strike slip fault. *Journal of Geophysical Re-*
961 *search: Solid Earth (1978–2012)* 86, 6067–6072.
- 962 Reif, D., Grasemann, B., Faber, R., 2011. Quantitative structural anal-
963 ysis using remote sensing data: Kurdistan, northeast Iraq. *AAPG*
964 *Bulletin* 95, 941–956.
- 965 Rosenau, M., Melnick, D., Echtler, H., 2006. Kinematic constraints
966 on intra-arc shear and strain partitioning in the southern Andes be-
967 tween 38 S and 42 S latitude. *Tectonics* 25.
- 968 Rutter, E., Hackston, A., Yeatman, E., Brodie, K., Mecklenburgh, J.,
969 May, S., 2013. Reduction of friction on geological faults by weak-
970 phase smearing. *Journal of Structural Geology* 51, 52–60.
- 971 Sieh, K., 1988. The Sunda megathrust- Past, present and future. *Geo-*
972 *logical Society of America Bulletin* 100, 1666–1703.
- 973 Sieh, K., 2007. The Sunda megathrust- Past, present and future. *Jour-*
974 *nal of Earthquake and Tsunami* 1, 1–19.
- 975 Sieh, K., Natawidjaja, D., 2000. Neotectonics of the Sumatran fault,
976 Indonesia. *Journal of Geophysical Research* 105, 28,29528,326.
- 977 Simoes, M., Avouac, J., Cattin, R., Henry, P., 2004. The Sumatra
978 subduction zone: A case for a locked fault zone extending into the
979 mantle. *Journal of Geophysical Research* 109, B10402.
- 980 Simons, W., Ambrosius, B., Noomen, R., Angermann, D., Wilson,
981 P., Becker, M., Reinhart, E., Walpersdorf, A., Vigny, C., 1999.
982 Observing plate motions in South East Asia: Geodetic results of
983 the GEODYSSSEA Project. *Geophysical Research Letter* 26, 2081–
984 2084.
- 985 Simons, W., Socquet, A., Vigny, C., Ambrosius, B., Haji Abu, S.,
986 Promthong, C., Subarya, C., Sarsito, D., Matheussen, S., Morgan,
987 P., et al., 2007. A decade of GPS in Southeast Asia: Resolving Sun-
988 daland motion and boundaries. *Journal of Geophysical Research:*
989 *Solid Earth* 112.
- 990 Socquet, A., Simons, W., Vigny, C., McCaffrey, R., Subarya, C., Sar-
991 sito, D., Ambrosius, B., Spakman, W., 2006. Neotectonics of the
992 Sumatran fault, Indonesia. *Journal of Geophysical Research* 111,
993 B08409.
- 994 Subarya, C., Chlieh, M., Prawirodirdjo, L., Avouac, J.P., Bock,
995 Y., Sieh, K., Meltzner, A.J., Natawidjaja, D.H., McCaffrey, R.,
996 2006. Plate-boundary deformation associated with the great Aceh-
997 Andaman earthquake. *Nature* 440, 46–51.
- 998 Suppe, J., 2014. Fluid overpressures and strength of the sedimentary
999 upper crust. *Journal of Structural Geology* 69, 481–492.
- 1000 Twiss, R.J., Moores, E.M., 1992. *Structural geology*. Macmillan.
- 1001 Unruh, J., Humphrey, J., Barron, A., 2003. Transtensional model for
1002 the Sierra Nevada frontal fault system, eastern California. *Geology*
1003 31, 327–330.
- 1004 Völker, D., Kutterolf, S., Wehrmann, H., 2011. Comparative mass bal-
1005 ance of volcanic edifices at the southern volcanic zone of the Andes
1006 between 33 S and 46 S. *Journal of Volcanology and Geothermal*
1007 *Research* 205, 114–129.
- 1008 Walter, T.R., Amelung, F., 2007. Volcanic eruptions following M 9
1009 megathrust earthquakes: Implications for the Sumatra-Andaman
1010 volcanoes. *Geology* 35, 539–542.

HIGHLIGHTS

- Helps our understanding in complex kinematics of an evolving strike-slip system
- Sumatran Fault System (SFS) kinematics resolved in its leading edge of deformation
- A fold-and-thrust belt (in western branch) and a Riedel system (in eastern branch)
- Compression (W) and tension (E) due to fracture mechanics of propagating fault tip